JOURNAL OF AIRCRAFT
Vol. 33, No. 5, September–October 1996

Investigation of the Unsteady Pressure Fluctuations on an F/A-18 Wing at High Incidence

B. H. K. Lee*
National Research Council, Ottawa, Ontario K1A 0R6, Canada
and
S. Marineau-Mes†
University of Ottawa, Ottawa, Ontario K1N 6N5, Canada

The results of an analysis performed on the unsteady pressure measurements taken from the wing of an instrumented rigid 6% scale model of the F/A-18 aircraft at high angles of attack are described. The experiment was carried out at the Institute for Aerospace Research 1.5-m trisonic blowdown wind tunnel. Space–time cross-correlations of the pressure field were performed on the wing upper surface using different reference transducers. The results are presented in the attached flow region on the inboard portion of the wing, which is under the influence of the leading-edge extension vortex system. The convection velocities of the broadband eddies were computed. The variation of the correlation contours of eddies along a typical skin-friction line is illustrated by an example.

Nomenclature

C_p	=	pressure coefficient
c	=	wing mean aerodynamic chord, 0.21 m
k	=	nondimensional frequency, fc/U
M	=	freestream Mach number
p	=	unsteady pressure
q	=	dynamic pressure
$R(x, y, \tau)$	=	cross-correlation function
$S_p(f)$	=	power spectral density
t	=	time
U	=	freestream velocity
x	=	distance measured along chord from a reference transducer
y	=	distance measured along span from a reference transducer
α	=	angle of attack
$\rho(x, y, \tau)$	=	normalized cross-correlation function
τ	=	time delay

I. Introduction

FLIGHT tests[1] have shown that the flow on the upper surface of the F/A-18 wing at high angles of attack is very complex. Using the oil-dots flow visualization technique,[2] the topology of the flow on the wing upper surface indicated that strong outflow dominated a major portion of the wing at M = 0.6 and α = 30 deg. It was found that flow separation occurred on a large area of the inboard leading-edge flap. The flow separated close to the leading-edge extension (LEX) and wing junction, and reattached on the flap. Separation also occurred along the hinge line with the flow reattaching a short distance behind it. Flow reversal on the inboard leading-edge flap was observed.

Presented as Paper 95-1865 at the 13th Applied Aerodynamics Conference, San Diego, CA, June 19–22, 1995; received July 25, 1995; revision received May 7, 1996; accepted for publication June 20, 1996.

*Group Leader, Institute for Aerospace Research, Experimental Aerodynamics and Aeroelasticity; also Adjunct Professor, Department of Mechanical Engineering. Associate Fellow AIAA.

†Graduate Student, Department of Mechanical Engineering.

Steady pressure measurements on the wing upper surface[2] revealed a low-pressure region on the inboard leading-edge flap that corresponded to the separated flow detected from the oil-dots visualization experiment. The pressure on a large portion of the wing surface was fairly uniform, rising gradually aft the hinge line towards the trailing edge.

Complementing the pressure measurements given in Ref. 2, spectral, space–time cross-correlation and coherence analyses of the unsteady pressure field on the upper surface of the F/A-18 wing were discussed in Ref. 3. The data were used to provide a model of the flow on the wing surface so that unsteady load for dynamic response studies, such as wing buffeting, on a flexible wing can be estimated. Further studies on the surface flow characteristics were carried out for different Mach numbers and angles of attack. These were reported in a recent paper.[4]

In this investigation, cross-correlation studies of the pressure field were carried out taking various transducers on the wing surface to be the reference and time correlations were performed with respect to the adjacent transducers. The tests were performed at three Mach numbers (M = 0.25, 0.6, and 0.8) and angles of attack between 25–35 deg. The surface flow results given in Ref. 4 show that for these Mach numbers and angles of attack, the flow is basically similar. In this article, only the results for M = 0.6 and α = 30 deg are presented, as space does not allow a discussion of M and α effects on the flow behavior. This investigation was carried out in the attached flow region on the inboard portion of the wing, which is under the influence of the LEX vortex system. The convection velocities at specific locations on the wing surface were computed and the velocity vectors give a convection pattern of the turbulent eddies. The correlation contours of broadband eddies were measured and their variations in space along a skin-friction line are shown to illustrate the change in the eddy dimension.

II. Wind-Tunnel Facility, Model and Data Acquisition

A. Wind-Tunnel Facility

The tests were performed in the trisonic blowdown wind tunnel at the Institute for Aerospace Research. The wind tunnel is a pressurized, intermittent flow facility, and is capable of operating in the subsonic, transonic, and supersonic flow re-

gimes. It has a Mach number range from $M = 0.1$ to 4.2. The walls of the 1.5 × 1.5 m transonic test section are perforated with 1.27-cm holes inclined 30 deg to the flow, allowing flow communication between the test section and a 3.65 m diam by 4.87 m length plenum chamber. The porosity of the walls is adjustable from 0.5 to 6%. For these tests, it was set at 4%. In subsonic and transonic tests, a hydraulically driven Mach number control system maintains the desired test section Mach number within ±0.003 as the model pitches, and the stagnation pressure can be held constant to an accuracy of ±137 Pa throughout the wind-tunnel run.

The test model was mounted on a cranked sting that forms part of the model support system. The strut can be programmed to move vertically and with the pitch linkage mechanism, the model angle of attack can vary from 0 to 33 deg. For high Mach number and dynamic pressure test conditions, aerodynamic loading causes bending of the sting, which can increase the angle of attack by up to 2 deg.

The tests were carried out at different Mach numbers and angles of attack, but only results at $M = 0.6$ and $\alpha = 30$ deg are presented in this article. The Reynolds number based on the model mean aerodynamic chord and the dynamic pressure corresponding to this Mach number are 3.38×10^6 and 27.2 kPa, respectively.

B. Model

The model used in this study is a rigid 6% scale model of the F/A-18. It consists of three major pieces: 1) an aluminum forebody with integral LEX and a single seat canopy, 2) a stainless-steel fuselage with integral wings, and 3) a stainless-steel rear fuselage. The center fuselage was bored to accept a 3.81-cm-diam six-component sting balance. AIM-9 missiles were mounted on the wingtips. For these experiments, the leading- and trailing-edge flaps were set at 34 and 0 deg, respectively. The horizontal stabilator angle was set at −9 deg. These angles correspond to the F/A-18 autoflaps up-mode schedule settings at high angles of attack. Boundary-layer transition trips were installed on the wings, LEX, fins, stabilators, and forebody of the model. A more detailed description of the model is given in Ref. 5.

The model starboard LEX and wing are instrumented with a total of 168 pressure transducers, 30 on the LEX and 138 on the wing. The position of these sensors is shown in Fig. 1, with an equal number on the upper and lower surface located directly opposite each other. The transducers are semiconductor sensors (Kulite XCQ-062-50A) with an active diameter of 0.88 mm and a frequency response in excess of 50 kHz. They were flush mounted in pockets that were machined on the wing surfaces. Trenches were also machined on the wing surfaces to accommodate the electrical wirings. The pockets were filled with a silastomer after the sensors were mounted, and this served the purpose of protecting the transducers. The trenches were filled with an epoxy compound and hand finished to the original wing profile.

Calibration of the pressure transducers was accomplished by mounting the F/A-18 model in a steel chamber with accurate pressure and temperature control. It was found that the transducers were sensitive to strain effects because of the deformation induced by the aerodynamic loading. The calibration procedure and the effects of strain are described in Ref. 2.

C. Data Acquisition

Wind-tunnel run conditions, model angle of attack, and other parameters were recorded at 100 Hz using a PDP 11/73 computer-based wind-tunnel data system. This computer system also controlled the wind-tunnel operation and model positions. A micro-Vax-based data acquisition system was used to collect data at a much higher sampling rate for unsteady pressure measurements. This data system consisted of a front end, a digital concentrator, and a parallel disk. The front end were blocks of instrumentation amplifiers, A/D converters, and filter/rms modules. The digital concentrator provided the link between the front end and the parallel disk. It accepted serial data from all of the A/D converters and transformed them to parallel data. The data could bypass the host computer and be written directly onto the disk through an interface port on the disk drive system. The sampling frequency was set at 38.4 kHz and the data system was capable of collecting up to 10 million samples per second. The parallel disk has a capacity of 6.5 Gbytes that was sufficient to hold data acquired from an average day's wind-tunnel runs. A typical wind-tunnel run generated approximately 400–600 Mbytes of data. The data were transferred onto 8-mm data cartridges overnight and the parallel disk was ready to accept data again the next day. Offline data processing was performed using HP 9000/750 and IBM RS/6000 workstations.

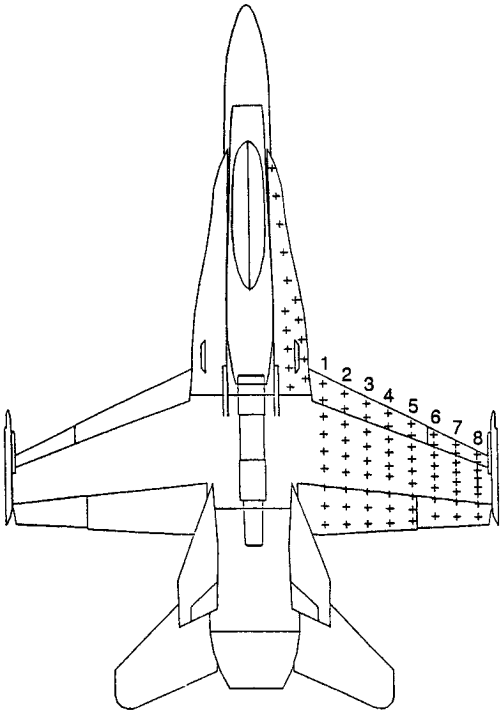

Fig. 1 Location of pressure transducers.

III. Results and Discussion

A. Surface Flow Studies

To understand the flow past the F/A-18 wing at high incidence, off-surface measurements or flow visualization are necessary. The flow is dominated by vortices that have their origins from the forebody, LEX, and wing. Mach number, angle of attack, and Reynolds number play an important role in the generation of these vortices and their subsequent effects on the flow past the wing.

The blowdown wind tunnel at the Institute for Aerospace Research (IAR) is not equipped with off-body flow visualization and quantitative pressure or velocity measurement devices. Off-body measurements are not feasible because the high dynamic pressure necessitates bulky instrument attachments that cause large disturbances to the flow. The results obtained in Refs. 2–4 are all obtained from surface measurements and they can, at best, give only a partial picture of the flow phenomena.

Surface flow visualization has been discussed in Refs. 2 and 4. In this section, the main observations from Ref. 2 for the test condition at $M = 0.6$ and $\alpha = 30$ deg are briefly outlined to give a general picture of the surface flow and the locations on the wing surface of the various regions where unsteady pressure measurements were analyzed. The main features deduced from the oil-dot streaks are shown in Fig. 2, but only

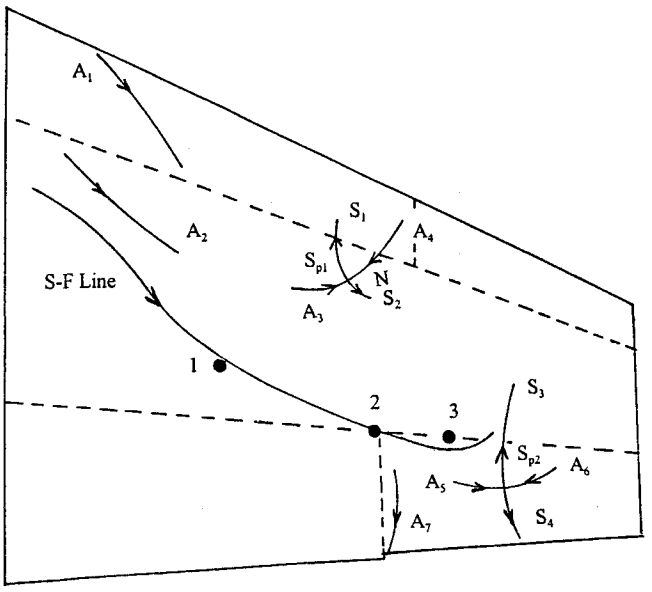

Fig. 2 Schematic of flow on wing upper surface at $M = 0.6$ and $\alpha = 30$ deg.

the separation and attachment lines are reproduced from the original oil-dots record.

At this angle of attack, the streamwise location of the primary LEX vortex burst[6] occurs slightly forward of the LEX fence leading edge. The attachment lines A_1 and A_2 indicate the locations where the flow reattaches after separating from the edge of the inboard leading-edge flap and the hinge line, respectively. Separation does not occur on the innermost portion of the flap because of the induced flow from the LEX. Aft of the line A_2, there is a small region where some oil streaks indicate converging flow. However, there is not sufficient detail from the oil-dots record to determine with certainty that local separation occurs. In general, the flow on the inboard leading-edge flap and in the region just aft of the flap behaves as reported in Ref. 1.

Inboard of the gap, formed between the leading-edge flaps and aft the hinge line, a saddle point S_{p1} is deduced. Converging towards the saddle point are the attachment lines A_3 and A_4. It is possible that A_3 is a continuation of A_2. However, this cannot be confirmed from the pattern of the skin friction lines. The pressure ratio across the gap is 0.62 and the flow is unchoked. Attachment line A_4 is induced by the vortex formed from the jet issuing from the gap. The location of A_4 on the inboard flap indicates that the local crossflow is in the inboard direction. Moving away from the saddle point S_{p1} are the separation lines S_1 and S_2. The skin friction lines that locate line S_1 show reversed flow on the wing and inboard leading-edge flap. This agrees with the results given in Ref. 1. The node N is identified by the rotating and converging skin friction lines that indicate a counterclockwise vortex. This vortex is also observed in Ref. 1. A second vortex[1] located behind the leading-edge hinge line on the inboard portion of the wing was not observed.

On the aileron, S_{p2} is formed by attachment lines A_5 and A_6 and separation lines S_3 and S_4. A large region of attached flow is seen and this lies between the wing root and the outer wing region bounded by S_3 and S_4 in the spanwise direction. Along the chordwise direction, the attached flow region is approximately located behind A_2 and downstream of S_{p1}, and ends at the trailing edge and inner aileron of the wing.

At the gap formed by the trailing-edge flap and the aileron, an attachment line A_7 is observed. For this angle of attack, the pressure ratio across the gap is 0.81. The location of A_7 on the aileron indicates that the local crossflow has an outward direction, as would be expected.

A skin friction line, marked S–F Line, deduced from the oil-dot streak lines is shown in Fig. 2. Also indicated in the figure along this line are the locations of three transducers labeled 1, 2, and 3, where analysis on the unsteady pressure measurements will be given in later sections. This is the region described by Fisher et al.[1] as the inboard portion of the wing that is under the influence of the LEX vortex system. The flow remains attached and the streamlines, in general, are directed outboard and aft.

B. Spectral Analysis

Spectral analysis of the pressure in various regions on the wing surface has been reported in Ref. 3. This article gives the spectral contents of the boundary layer in the region of the inboard wing with attached flow for the three transducers marked in Fig. 2. Previous studies[3] have shown that the shape of the spectra can be quite different on the leading-edge flaps and the outer wing. However, on the main wing, where the present studies are being conducted, some variations are expected, but in general, the spectral shapes show similar characteristics.

The power spectral density (PSD) of a time series $p_i(t)$, decomposed into K intervals, is defined by the following equations:

$$S_p(f) = \frac{1}{KN} \sum_{i=0}^{K-1} S_i(f) \tag{1}$$

$$S_i(f) = |P_i(f)|^2 \tag{2}$$

where $P_i(f)$ is the finite Fourier transform of $p_i(t)$, and N is a factor that depends on the smoothing window used.

These equations are expressed in a form described in Ref. 7 for easy implementation of the fast Fourier transform (FFT) algorithm. The discretely sampled input data typically represents approximately 10 s of data, which gives close to 400,000 points. The FFT length was set at 8192 points, and the frequency resolution is slightly less than 5 Hz. A Hamming window was applied to the data, and an overlap of 50% between segments was selected. The number of averages for the computation of the PSD was approximately 190.

The frequency in Hz is converted to k in the PSD plots. This is obtained by multiplying the frequency by a characteristic time scale that is equal to the ratio of the wing mean aerodynamic chord to the freestream velocity.

The spectral shapes shown in Fig. 3 are fairly typical of those measured on airfoils at high subsonic Mach numbers and

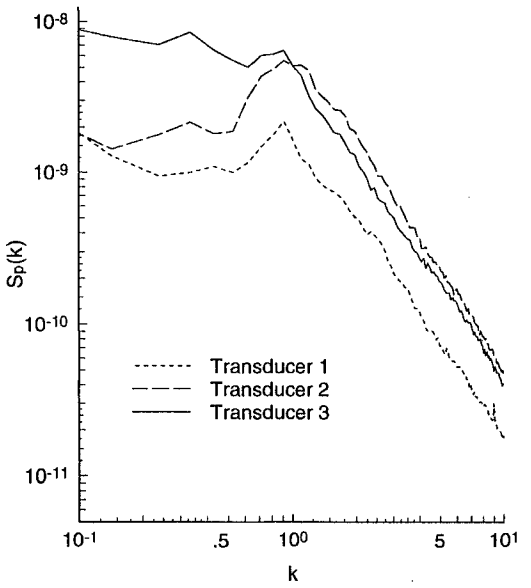

Fig. 3 Power spectral densities.

Reynolds numbers. They show the spectrum to be fairly flat or falling gradually with decreasing frequency at low frequencies for $k < 1$. They fall off rapidly with increasing frequency at frequencies higher than this value of k. The high-frequency region where the spectrum is falling off still accounts for a large portion of the total pressure energy. In buffet and dynamic response studies, the low-frequency energy spectrum is more important and usually it is sufficient to consider frequency below 2 kHz. This was the reason that Ref. 3 did not give results above $k = 2$. However, the results presented in this article extend up to a frequency of 10 kHz and are of interest in the study of the turbulent structure of the flow in the boundary layer.

The curves at high frequencies shown in Fig. 3 are very similar for transducers 2 and 3. They are shifted upwards from the curve for transducer 1. It is seen that as an eddy convects downstream across the wing, its energy content increases. However, along some skin-friction lines (e.g., near the trailing edge), this is not necessarily true. The increase is larger at lower frequencies. At the high-frequency range of the spectra, the slope $n = \mathrm{d}[\ell n\, S_p(k)]/\mathrm{d}[\ell n\, k] = -2$ for the three curves. Various authors[8] have reported different values of n for airfoils and wings, depending on the type of flow under consideration.

Previous investigations[5] of the unsteady pressure on the vertical fin and in the flowfield behind it showed that at high angles of attack, the power spectral densities exhibit a broadband peak with centered k between 0.45–0.5. The limited amount of pressure spectra reported in Ref. 2 did not indicate a frequency in the pressure signature on the wing that may be attributed to the burst vortex. The value of k determined from the vertical fin experiments was computed using the fin mean aerodynamic chord (0.127 m) as the characteristic length. The value of k corresponding to $c = 0.21$ m used in this investigation would be between 0.74–0.82. Transducers 1 and 2 in Fig. 3 show a broad peak near $k = 1$. It cannot be said for certain that this peak is related to the burst vortex, since transducer 3, which is close to transducer 2, did not show this frequency behavior. Further analysis is needed to relate the spectra on the LEX close to the vortex burst with that on the wing. This can be achieved by performing correlation studies between the pressure time histories on the LEX and wing. Some preliminary studies have been carried out, but they will not be reported herein.

C. Space–Time Cross Correlation

The cross-correlation function of two time series, say pressure p, at two points in space is defined as

$$R(\Delta x, \Delta y, \tau) = \overline{p(x, y, t) \cdot p(x + \Delta x, y + \Delta y, t + \tau)} \quad (3)$$

where Δx and Δy are the spatial separations between the two pressure measurements. The Institute of Electrical and Electronics Engineers coherence and cross-spectral estimation algorithm[7] was used to perform the broadband correlation of the discrete time series. Results are usually expressed in nondimensional form given by the following expression:

$$\rho(\Delta x, \Delta y, \tau) = \frac{R(\Delta x, \Delta y, \tau)}{[R(x, y, 0) \cdot R(x + \Delta x, y + \Delta y, 0)]^{1/2}} \quad (4)$$

This function has a range $-1 < \rho(\Delta x, \Delta y, \tau) < 1$.

1. *Cross-Correlation Contours*

The intention of this wind-tunnel program was to provide loads for structural analysis of the wing and center fuselage for the International Follow-On Structural Test Program (IFOSTP) between Australia and Canada. The locations of the transducers for this investigation are, therefore, chosen to satisfy the IFOSTP requirements and may not be adequate for investigating the flow characteristics in some regions on the wing surface. This is mainly because of the insufficient spatial resolution in analyzing the flow in the various separation and reattachment regions that are small compared to the transducers' grid. The small size of the 6% model and the expenses and difficulties in the installation of a large amount of transducers preclude the addition of any more sensors than are already installed on the wing. Note that the attachment and separation lines in Fig. 2 are obtained from oil-dots placed 10 mm apart, except at the leading edge and in the vicinity of the tip missile where the spacing is reduced to 5 mm. Even with this close spacing of the oil-dots, there are some regions of the flowfield where changes are rapid and finer oil-dots spacing is desirable.

Cross-correlation studies were carried out by taking each transducer on the wing surface to be the reference and performing time correlations with respect to the adjacent transducers using Eq. (4). The results show that at $M = 0.6$ and $\alpha = 30$ deg, pressure correlation is found to be good in large regions on the inboard wing and trailing-edge flap, and also on the outboard wing and aileron. These two regions are separated by S_3 and S_4.

On the leading-edge flaps along rows 1 and 2 in the spanwise direction (Fig. 1), correlation is detected only in small local regions on the leading-edge flap. The decay of the correlation function is slightly longer, which suggests that some lower frequency phenomenon dominates the flow.

Along chordwise rows 2, 3, and to a certain extent row 4, the flow on the leading edge and slightly behind the hinge line exhibits poor correlation. This is to be expected since surface flow visualization[2] indicated the flow to be very complicated with separation and reattachment on the inboard leading-edge flap. However, beyond the hingeline, good correlation is observed after the flow reattaches. In transducer rows 5–8, correlations extend spatially for a large percentage of the chord. It was found that poor correlation is generally detected across attachment and separation lines.

An example of the space–time cross-correlation map for the seventh spanwise row of transducers, using transducer 2 marked in Fig. 2 as the reference, is given in Fig. 4. The isocorrelation lines are swept forward and show that correlation extends for fairly large distances along the span. The slope of the line joining the peaks of the contours gives the convection velocity in the spanwise direction. Ideally, a coordinate system should be chosen so that one of the axes will be aligned with the eddy path and the slope thus obtained will be the true convection velocity. The envelope of the correlation function decays to a value of 0.1 or less in approximately 1 ms.

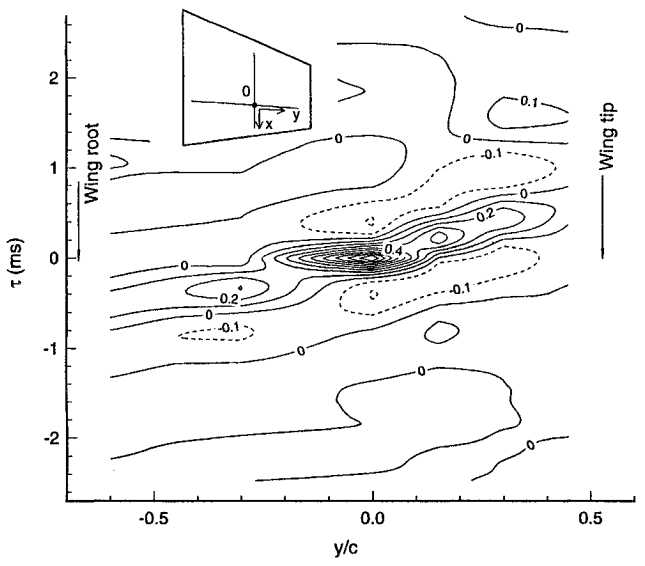

Fig. 4 Cross-correlation coefficient contours at transducer 2 along spanwise direction.

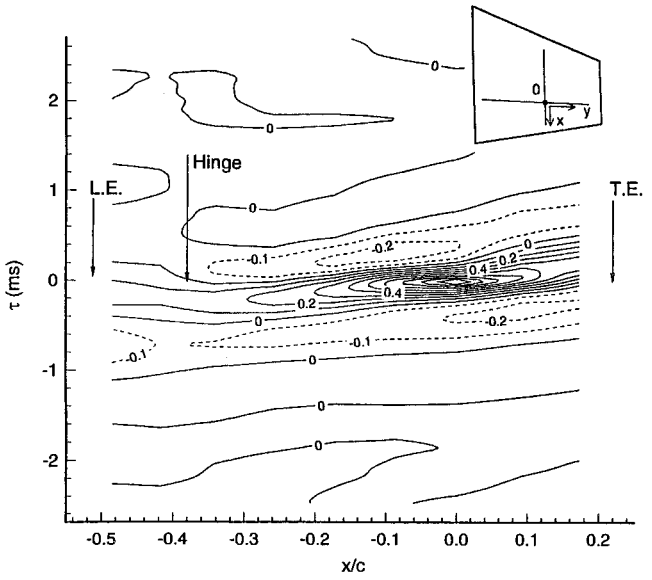

Fig. 5 Cross-correlation coefficient contours at transducer 2 along chordwise direction.

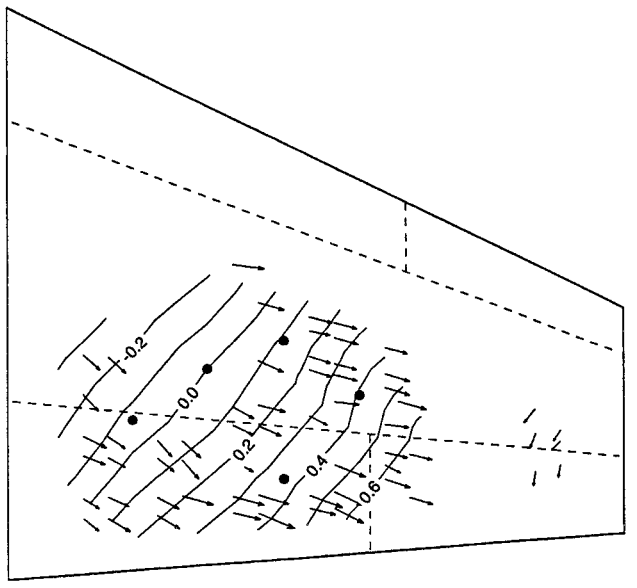

Fig. 6 Peak correlation delay contours: $M = 0.6$ and $\alpha = 30$ deg.

Figure 5 shows the cross correlation along the fifth row of chordwise transducers using the same reference transducer as in Fig. 4. The chordwise spatial correlation is seen to extend for quite large upstream and downstream distances. Beyond the leading-edge hinge line, the correlation is not too meaningful. Similar to the spanwise correlation function, the correlation function envelope along the chordwise direction decays to values of 0.1 or less after 1 ms. The peak correlation contour lines are not swept forward in a time scale like the spanwise correlation. The small slope indicates the convection velocity component in the downstream direction to be small.

Note that the spacings of the transducers are not sufficiently small to give good spatial resolutions. The large number of contour lines close to the reference transducer in Fig. 4 is obtained using three transducers spaced approximately 0.3 and $0.15c$ apart from the reference, whereas in Fig. 5, they are both $0.1c$ on either side of the reference transducer. Hence, the contours are only approximate and subject to errors.

2. Convection Velocity

Using transducer 6 on the third chordwise row as reference, Ref. 2 computed the cross-correlation functions with all other transducers. The cross-correlation plots that exhibited a clear peak were selected and the peak correlation time delay was recorded. The data were then used to generate a map of peak correlation time delay contours. A large region of correlated pressure fluctuations was found on the wing behind the hinge line, and this corresponds to the attached flow region from the oil-dots visualization studies.[2] Using different reference transducers, similar maps can be constructed. It was shown that the peak correlation time delay contour lines overlap each other. Figure 6 gives the contour lines averaged from individual sets obtained from five transducers whose positions are marked in the figure. The delay time in milliseconds was shifted using the sixth transducer on the third chordwise row as the reference, and the value of τ is set to 0 along the peak contour passing through this transducer. In this region, the convection of the eddies can be determined at any position on the wing surface, using the time delays obtained from this figure.

Depending on the location on the wing, the convection velocity computed varies from 120 to 155 m/s. This corresponds to values of $0.59-0.76U$, respectively.

Superimposed in Fig. 6 are local convection velocities calculated at different positions. These are denoted by vectors placed at the centroid of the triangle formed by three transducers. Assuming that the flow convection front is straight and

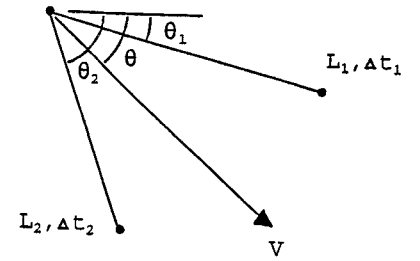

Fig. 7 Schematic of calculating convection velocity from three transducers.

that it travels at a constant velocity, the convection front velocity and direction in an area between three transducers can be estimated. For the calculations, the time delays and distances between any one transducer and the other two transducers are assumed to be known. Taking the case of three transducers as positioned in Fig. 7, the direction of propagation of the convection front is solved with the following equation:

$$\frac{L_1 \cos(\theta - \theta_1)}{\Delta t_1} = \frac{L_2 \cos(\theta - \theta_2)}{\Delta t_2} \tag{5}$$

Once θ is known, the convection front velocity can be determined from this equation. The criterion in calculating the velocity at each point is that the correlation function is well behaved and its peak value is greater or equal to 0.2. The velocities calculated from this method vary between 120–160 m/s, and the range of values is similar to that determined from Fig. 6. Note that the vectors from some of the transducers close to each other may not be pointing in the direction as expected. This is because of the errors introduced when Δt is small and of the order of a few sampling intervals. The accuracy can be improved by increasing the sampling rate of the times series. This was not carried out because of the already large amount of data collected from each wind-tunnel run, making data management more cumbersome.

The analysis is based on the assumption that the flow is semifrozen and the convection velocity is the weighted average of many eddy velocities. Space–time correlations of boundary layers on flat plates have shown that the convection velocities determined from measurements depend on the spatial separations of the transducers. It can vary from 0.55 to 0.85 of the freestream velocity for very small measuring distance to large

separations. This is attributed to the fact that, for small separations, the convection is dominated by small eddies close to the wall, traveling relatively slower. For large separations, these eddies will have decayed, leaving the faster-moving large-scale eddies to determine the convection velocity. However, there are insufficient transducers installed in the present wind-tunnel model to investigate this effect. For nonfrozen pattern, the eddies move with a variety range of velocities depending on the frequency decomposition of the eddy. These velocities can be determined in a similar fashion by using narrowband cross correlations. This has not been carried out, and only broadband convection results are given in this article.

3. Broadband Eddy Convection

The correlation functions at zero time delay $\rho(0, \Delta y, 0)$ and $\rho(\Delta x, 0, 0)$ corresponding to Figs. 4 and 5 are shown in Figs. 8 and 9. Define two length scales in the x and y directions as

$$L_{\Delta x} = \int_0^\infty \rho(\Delta x, 0, 0)\, d\Delta x \tag{6}$$

$$L_{\Delta y} = \int_0^\infty \rho(0, \Delta y, 0)\, d\Delta y \tag{7}$$

The values of $L_{\Delta x}$ and $L_{\Delta y}$ are approximately $0.1c$, showing that the length scales are similar in both directions. At this reference transducer, the convection velocity determined from Fig. 6 is $0.65U$. The time scale of an eddy is estimated to be 0.16 ms. This value is only approximate and assumes that the eddy convection direction coincides with the y axis as shown in the inset in Fig. 4. The corresponding values of $L_{\Delta x}$ and $L_{\Delta y}$ at transducers 1 and 3 are 0.12, $0.12c$, and 0.1, $0.075c$, respectively. The time scales are 0.16 and 0.12 ms.

The correlation contours $\rho(\Delta x, \Delta y, 0)$ on the wing surface are shown in Figs. 10–12 at the three transducers marked in Fig. 2 along a skin-friction line. Only positive values with a minimum of 0.1 are shown. These figures give a two-dimensional description of the spatial extent of an eddy.

The steady-state C_p measurements are superimposed in Figs. 10–12 to aid in the interpretation of the results presented for the correlation contours. Since the flow is highly unsteady, the steady pressure was obtained by averaging the pressure time series that were 10 s in duration. To be able to deduce an approximate map of the pressure field on the wing, it was decided to present the steady-state pressure data in the form of contour plots. The commercially available TECPLOT was used with parameters set at the default values and some smoothing was allowed. It should be pointed out that different

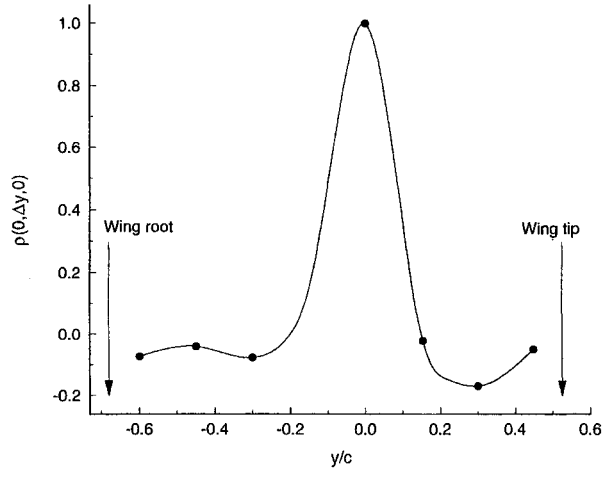

Fig. 8 $\rho(0, \Delta y, 0)$ for transducer 2 along spanwise direction.

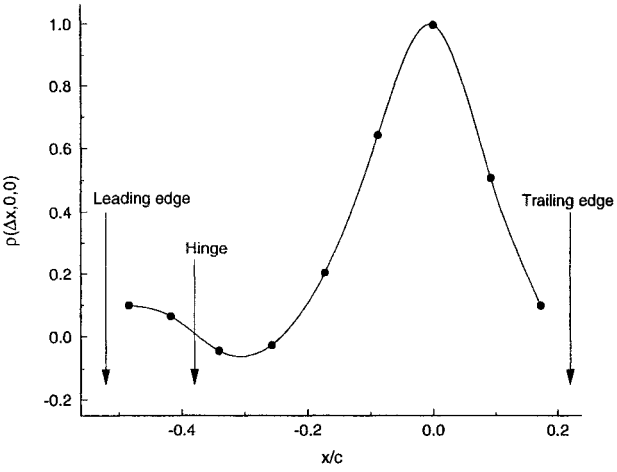

Fig. 9 $\rho(\Delta x, 0, 0)$ for transducer 2 along chordwise direction.

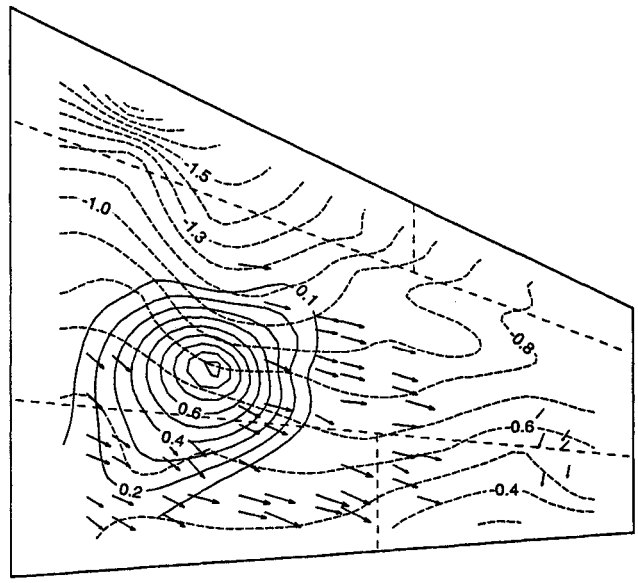

Fig. 10 Correlation contours at transducer 1: M = 0.6 and α = 30 deg.

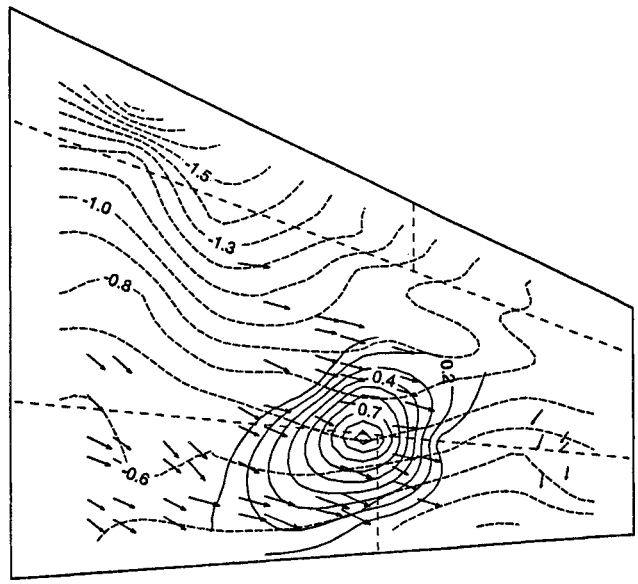

Fig. 11 Correlation contours at transducer 2: M = 0.6 and α = 30 deg.

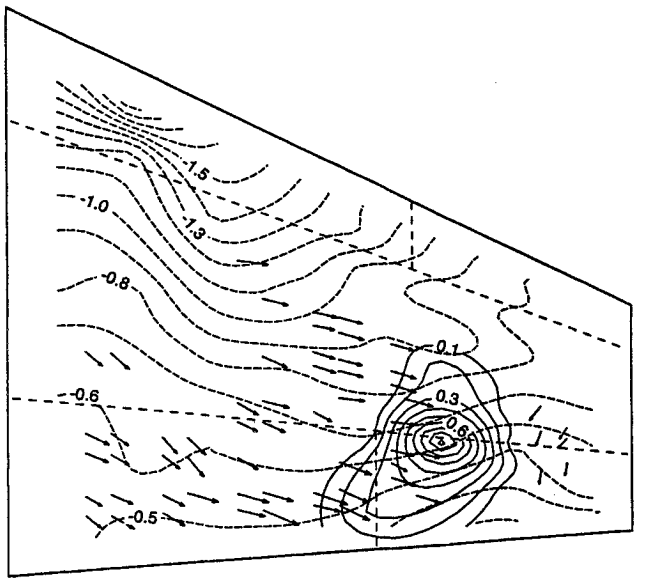

Fig. 12 Correlation contours at transducer 3: M = 0.6 and α = 30 deg.

plotting packages may give slightly different contour lines depending on the interpolation scheme chosen. It is not possible to ascertain the accuracy of the contour lines since the data are interpolated from grid-measurements and all sharp variations are smoothed out. The contours can represent at best some average or overall distributions of the pressure.

In Fig. 10, it can be seen that the pressure contours aft of the leading-edge inboard flap hinge line follow closely to the shape of the attachment lines A_2 and A_3. The region formed by joining these two lines probably encloses the separated flow behind the hinge line. On the leading-edge flaps, a positive pressure gradient in the outboard direction is detected. In the vicinity of the two saddle points S_{p1} and S_{p2}, the contours show a small abrupt change at the separation lines.

The eddies are distorted as they are convected across the wing along the path shown in Fig. 2, which is close to one of the constant C_p contours. The correlation contours are more compressed in the direction of the skin-friction line although the pressure gradient is much less than that normal to it. For example, at transducer 2, the value of C_p varies from -0.9 behind the leading-edge hinge line to -0.5 close to the trailing edge on the 0.2 contour line. At transducer 3, the eddy is smaller than that at transducer 2, and its shape is more distorted in the outflow direction. The correlation line at 0.1 is very close to the limit of the region on the wing where the outflow from the wing root meets the flow from the missile launcher. The dividing line is given by S_3 and S_4 shown in Fig. 2. All of the contours on the right of transducer 3 in Fig. 12 used values from transducer row 7 and are under the influence of the flow from the wingtip. The contours to the left are not affected by the outer wing region.

The definitions of eddy size as given in Eqs. (6) and (7) assume the flow region under consideration to be sufficiently large compared to the size of an eddy. In this case, the length scales can be evaluated satisfying the limits in the integrals. In considering flow past a finite wing, errors will be introduced in the calculation of the length scales when the large eddies are not small compared to the dimensions of the wing planform. Also, the presence of various flow regions makes it difficult to determine these scales accurately. The results provided in this article only serve to give an estimate of the dimensions of these large eddies using the standard cross-correlation techniques in boundary-layer studies.

Conclusions

The flowfield on the wing upper surface of a rigid 6% scale model of an F/A-18 was investigated from analyses of the PSD and broadband space–time cross correlations from a large number of transducers spaced in a grid manner on the wing. In particular, the convection of large eddies in the attached flow region on the inner portion of the wing that is under the influence of the LEX vortex system has been studied in some detail.

The envelope of the cross-correlation function between most of the transducers decayed to values of 0.1 or less in approximately 1 ms. The transducers across separation and reattachment lines usually exhibit poor correlation.

Using the peak cross-correlation time delays constructed from a number of reference transducers, the convection velocities of the broadband eddies on the wing surface were determined. Their values agree reasonably well with those calculated at specific locations using groups of three transducers. The correlation contours of an eddy following a skin friction line were determined to illustrate the distortion of an eddy as it convected toward the outer wing. Estimates of the length scales at three transducer positions are given. The inaccuracies in determining length scales for eddies large compared to the wing planform or where different types of flow coexist are pointed out.

Acknowledgments

The authors wish to acknowledge the financial support from the Institute for Aerospace Research, the Department of National Defence, and the Natural Sciences and Engineering Research Council of Canada.

References

[1]Fisher, D. F., Del Frate, J. H., and Richwine, D. M., "In-Flight Flow Visualization Characteristics of the NASA F-18 High Alpha Research Vehicle at High Angles of Attack," NASA TM 4193, May 1990.

[2]Lee, B. H. K., Valerio, N. R., and Tang, F. C., "Steady and Unsteady Pressure Distributions on an F/A-18 Wing at α = 30 Deg," *Journal of Aircraft*, Vol. 31, No. 4, 1994, pp. 862–867.

[3]Lee, B. H. K., and Marineau-Mes, S., "Investigation of the Unsteady Pressure Fluctuations on an F/A-18 Wing at High Incidence," AIAA Paper 95-1865, June 1995.

[4]Lee, B. H. K., and Marineau-Mes, S., "Mach Number and Angle of Attack Effects on the Flow Past a Fighter-Type Wing at High Incidence," AIAA Paper 96-2510, June 1996.

[5]Lee, B. H. K., and Brown, D., "Wind-Tunnel Studies of F/A-18 Tail Buffet," *Journal of Aircraft*, Vol. 29, No. 1, 1992, pp. 146–152.

[6]Erickson, G. E., Hall, R. M., Banks, D. W., Del Frate, J. H., Schriener, J. A., Hanley, R. J., and Pulley, C. T., "Experimental Investigation of the F/A-18 Vortex Flows at Subsonic Through Transonic Speeds, Invited Paper," AIAA Paper 89-2222, July 1989.

[7]Rabiner, L. R., Schafer, R. W., and Dlugos, D., "Chapter 2.1, Periodgram Method for Power Spectrum Estimation," "Chapter 2.3, a Coherence and Cross Spectral Estimation Program," *Programs for Digital Signal Processing*, edited by the Digital Signal Processing Committee, IEEE Acoustics, Speech and Signal Processing Society, Inst. of Electrical and Electronics Engineers, New York, 1979.

[8]Hwang, C., and Pi, W. S., "Investigation of Steady and Fluctuating Pressure Associated with the Transonic Buffeting and Wing Rock of a One-Seventh Scale Model of the F-5A Aircraft," NASA CR 3061, Nov. 1978.